Wearable 3D-Printed Thumb-Shaped Device Based on Fiber Bragg Grating Sensor for Epidural Space Detection

Francesca De Tommasi, *Student Member, IEEE*, Carlo Massaroni, *Senior Member, IEEE*, Michele Arturo Caponero, Emiliano Schena, *Senior Member, IEEE*, Daniela Lo Presti, *Member, IEEE*, and Massimiliano Carassiti

***Abstract*—Fiber Bragg grating sensors (FBGs) are increasingly popular in various biomedical fields due to their undeniable benefits, hardly found in other sensing technologies. To overcome FBGs' inherent fragility, encapsulation in other hosting materials, such as silicone rubber or resins, has been widely practiced. This approach allowed for high flexibility and adaptability of the developed devices but can be time-consuming and labor-intensive. Fused deposition modeling (FDM) has recently been proposed to develop 3D-printed devices embedding FBGs, enabling the deployment of systems with high repeatability, accuracy, and fast fabrication time. The exploitation of 3D-printed device based on FBG for biomedical applications is still little explored in the literature. In this article, we proposed an application never yet investigated to assist physicians in performing epidural procedures. Accurately detecting the epidural space (ES) in these treatments is highly challenging as it relies on the clinician's perception. Moreover, due to ES small size, the risk of failure is common in clinical practice. In this field, state-of-the-art solutions have been devised to instrument the generally used needle or the syringe plunger. These solutions can obstruct the drug delivery inside the needle or contaminate the sterile field. In this study, we propose a 3D-printed thumb-shaped device embedding a single FBG conceived to be worn under a clinician's glove, thus overcoming the limitations associated with the existing systems. Design, fabrication, and metrological characterization of the proposed system are reported. Furthermore, a feasibility assessment in a real clinical scenario demonstrated its ability to detect the ES correctly.**

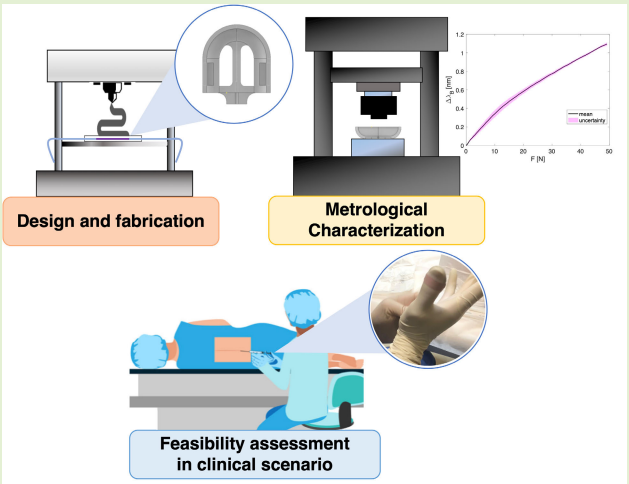

***Index Terms*—3D printing, epidural space (ES), fiber Bragg grating sensor, loss of resistance (LOR), thumb-shaped device.**

Manuscript received 6 June 2023; accepted 10 June 2023. Date of publication 19 June 2023; date of current version 1 August 2023. The associate editor coordinating the review of this article and approving it for publication was Prof. Arnaldo G. Leal-Junior. *(Daniela Lo Presti and Massimiliano Carassiti contributed equally to this work.) (Corresponding author: Daniela Lo Presti.)*

This work involved human subjects or animals in its research. Approval of all ethical and experimental procedures and protocols was granted by the Institutional Ethics Committee of Università Campus Bio-Medico di Roma under Reference No. 04.16-OSS, and performed in line with the Declaration of Helsinki.

Francesca De Tommasi, Carlo Massaroni, Emiliano Schena, and Daniela Lo Presti are with the Unit of Measurements and Biomedical Instrumentation, Departmental Faculty of Engineering, Università Campus Bio-Medico di Roma, 00128 Rome, Italy (e-mail: d.lopresti@unicampus.it).

Michele Arturo Caponero is with the ENEA Frascati Research Center, Frascati, 00044 Rome, Italy.

Massimiliano Carassiti is with the Fondazione Policlinico Universitario Campus Bio-Medico, 00128 Roma, Italy, and also with the Research Unit of Anesthesia, Intensive Care and Pain Management, Department of Medicine and Surgery, Università Campus Bio-Medico di Roma, 00128 Roma, Italy.

Digital Object Identifier 10.1109/JSEN.2023.3286284

I. Introduction

OVER the past decades, fiber Bragg Grating sensors (FBGs) are gathering increasing consideration for sensing applications in a plethora of biomedical fields [1], [2], [3]. Solutions based on both silica and polymer optical fibers can be found in [1], [4], and [5]. FBGs' ongoing popularity stems from a series of qualities hardly to be found in other competitors (e.g., electrical sensors). Their biocompatibility, small size, lightweight, nontoxicity, stability over a long period, immunity to electromagnetic interferences, and multiplexing capabilities for silica FBGs have encouraged their spread beyond other technologies [6]. As a plus, their sensitivity to both strain and temperature broadens their application for measuring multiple parameters of importance in medical treatments and disorders' diagnoses [7], [8], [9], [10], [11], [12], [13].

However, the inherent fragility of silica FBGs represents one of the main shortcomings of these sensors. In the past

years, several research groups have extensively explored the enclosing of FBGs in other hosting materials to overcome this limitation. So far, silicone rubbers or resins have proved suitable for this purpose. Using these materials enables the customization of smart systems with high flexibility and adaptability [10], [12], [14], [15], [16]. Notwithstanding, several steps involved in the fabrication process, such as the design and engineering of the mold to shape the sensing elements as desired or the period required to cure the polymeric matrix, can be time-consuming and labor-intensive [17]. Recently, the growing success of 3D printing technology paved the way for integrating FBGs within 3D-printed devices [18], [19]. The exploitation of fused deposition modeling (FDM) allows for the development of FBG-based systems with high repeatability, precision, and low cost. This approach has been barely explored in biomedical applications since the leading-edge solutions account for a small fraction [20], [21], [22], [23]. Here, we propose a new application not yet explored to support clinicians in performing epidural procedures. These treatments foresee the supply of anesthetics and/or steroids into the epidural space (ES) [24], [25]. The drug administration is achieved through the insertion of a specific needle (i.e., Tuohy needle) between two vertebrae, crossing different tissues until reaching the ES. However, the small size of the ES (between 2 and 6 mm) poses a more challenging and failure-prone procedure [26]. So, accurate detection of the ES is critical to successfully performing the treatment and avoiding potential complications for patients. The most common method to identify the ES is the loss of resistance (LOR) technique which can be performed by filling the syringe with saline solution or air for allowing the needle advancement [27]. LOR foundation lies in different densities of tissues' piercing, particularly the ligamentum flavum (i.e., hard tissue) and the ES (i.e., soft tissue). The density difference is related to the variable force necessary to push the syringe plunger for allowing needle advancement. During the needle penetration, the force reaches a maximum value at the level of the ligamentum flavum. On entering ES, there is a rapid drop in force values perceivable by the operator. The epidural procedure is usually performed in a blind manner and is dependent on the clinician's perception. For this reason, the procedure's failure occurs commonly in clinical practice [28], [29]. In the literature, several proposed systems have demonstrated the capability of FBG sensors to detect the ES successfully, thus providing guidance to the clinician during the procedure [30], [31], [32], [33], [34], [35], [36]. The majority of the proposed solutions are intended to instrument Tuohy's needle [30], [31], [32], [33]. However, the main inconveniences connected with these technologies include possible occlusion for drug delivery, the inability of multiple uses because the Tuohy needle is disposable, and, in some cases, alteration of the normal procedure, which inevitably involves a training period for the operator. More recently, our research group proposed the design and optimization of an FBG-based soft system conceived to fit the syringe plunger [34], [35], [36]. This device allows for overcoming the weaknesses of the instrumented needle but requires proper sterilization before every use.

The present study aims to address the limitations associated with the existing state-of-the-art systems by leveraging the latest advancements in 3D printing technology and the well-known benefits of FBG technology to develop a wearable 3D-printed device for LOR detection. The proposed solution offers several advances, including an easily customizable design, increased stability and robustness, and high cost-effectiveness. For the first time, a device for LOR detection is designed to be worn under the clinician's glove, thus preventing contamination of the sterile field or impairment of drug release during epidural procedures. We report the proposed system's design, fabrication, and metrological characterization. Finally, a feasibility assessment in a real clinical scenario is presented, demonstrating its ability to detect ES correctly.

II. Design and Fabrication of the Wearable 3D-Printed Thumb-Shaped Device Based on FBG Technology

The remainder of this section is the following. First, a description of the working principle of the 3D-printed thumb-shaped device based on FBG is detailed, considering the scenario of interest. Then, information on the system design and dimensions is provided. Finally, the fabrication process based on FDM technology is described.

A. 3D-Printed Thumb-Shaped Device: Working Principle

The thumb-shaped proposed device is based on FBG technology. An FBG is a resonant structure inscribed in a short segment of an optical fiber core capable of reflecting particular wavelengths of light and transmitting all others. This function is achieved by permanent periodic variation in the refractive index along the propagation axis resulting in a wavelength-specific reflector. Once an incident broadband light signal crosses an optical fiber and hits the grating, a narrow spectrum centered around the so-called Bragg wavelength (i.e., λ_B) is back-reflected, satisfying the following condition [37]:

$$\lambda_B = 2 \cdot n_{\text{eff}} \cdot \Lambda. \tag{1}$$

FBG's operating principle is based on a shift in λ_B (i.e., $\Delta\lambda_B$) occurring when the fiber is subjected to strain (i.e., ϵ) or temperature variations (ΔT), according to the equation below:

$$\frac{\Delta\lambda_B}{\lambda_B} = (1 - \rho_\epsilon) \cdot \epsilon + (\alpha_\Lambda + \alpha_n) \cdot \Delta T \tag{2}$$

where ρ_ϵ is the strain coefficient, ϵ is the strain along the longitudinal axis of the fiber, α_Λ is the thermal expansion coefficient, and α_n is the thermo-optic coefficient.

In this case, the influence of ΔT can be considered negligible compared with the contributions due to ϵ caused by the anesthesiologist's applied force on the syringe plunger. In detail, during epidural procedures, the FBG sensor embedded in the printing material is expected to experience strain when the clinician's thumb applies the force to advance the needle. Once the needle bypasses the ligamentum flavum and reaches the ES, the grating releases since the LOR occurs.

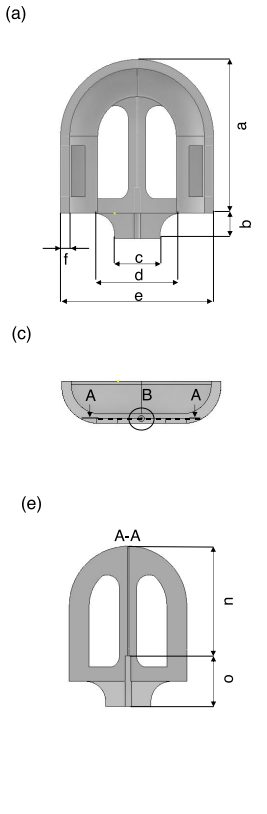

Dimensions [mm]	
a	30.1
b	5.0
c	9.6
d	16.7
e	30.0
f	2.5
g	10.0
h	3.0
i	1.2
l	0.24 (Ø)
m	0.30
n	21.4
o	10.0

Fig. 1. CAD of the wearable thumb-shaped device from (a) frontal and (b) and (c) lateral views. (d) and (e) Details of the two channels. All the main dimensions are reported in the table.

This event can be displayed on the recorded FBG signal as a sudden drop in $\Delta\lambda_B$.

B. Device Design

In this study, the FBG sensor was conceived to be embedded in a thumb-shaped 3D mold. A CAD software (i.e., Autodesk Inventor) was used to engineer the desired shape for the proposed system, accounting for two main requirements: 1) a biomimetic shape to fit the anesthesiologist's thumb and 2) reduced dimensions to minimize the invasiveness since it is conceived to be worn under the clinician glove. Compared with other works in the literature, the sensing solution proposed in the present study has two main advantages: it prevents contamination of the sterile field and obstruction for drug release during this type of procedure compared with other solutions based on needle or syringe plunger instrumentation and makes easy the device customization improving the adaptability to the anesthesiologist thumb and the robustness of the FBG enclosed at the specimen core.

The proposed system had a total length of 35.1 mm [a and b in Fig. 1(a)], a width of 30 mm [e in Fig. 1(a)], and a thickness of 2.5 mm [f in Fig. 1(a)]. To embed the FBG sensor during the printing process, a grooved rectangular-shaped channel was included in the structural design. It consisted of a base of 0.3 mm and a height of 0.24 mm [details reported in Fig. 1(d)], vertically constructed to allow the passage of the optical fiber under the sterile glove and its subsequent connection to the optical interrogator without impairing the anesthesiologists' movements during the procedure. Two openings on the interfacing surface allowed for increasing the tactile sensation of the clinician's thumb on the plunger [as shown in Fig. 1(a)]. An acrylate-coated FBG 5 mm in length (λ_B equal to 1557 nm and reflectivity value of 84.61%) was selected to develop the proposed device. The choice of a 5-mm FBG is warranted because longer FBG lengths are marked by a more prominent peak in the reflected spectrum, which results in a higher signal-to-noise-ratio, thus ensuring better accuracy in peak detection and the estimation of $\Delta\lambda_B$ shift [38], [39]. Moreover, the use of 5-mm FBG instead of sensors with higher grating lengths allowed us to find the best compromise between performance and device encumbrance. To improve the optical fiber robustness, two main solutions were adopted: 1) the optical fiber was placed inside a flexible tube of 900 μm, except for its sensitive portion (i.e., 5 mm) and partially embedded in the device during the printing process through another dedicated grooved channel [o in Fig. 1(e)] concentric to the first one and 2) in correspondence with the FBG exit point, a support structure [dimensions indicated with b, c, and d in Fig. 1(a)] was designed to gently guide the optical fiber and avoid abrupt changes in direction. Finally, as can be seen from Fig. 1(a) and (b), two lateral holes [dimensions denoted with g and h in Fig. 1(b)] were designed for the insertion of an elastic band for wearing the thumb-shaped device. All the dimensions are listed in the table of Fig. 1.

TABLE I
PRINTING SETTINGS

Printing parameters	Set value
Infill density	30%
Infill pattern	Lines
Printing temperature	228 °C
Printing speed	15%

C. Printing Settings and Fabrication Process

FDM was chosen for developing the thumb-shaped device by means of a 3D printer (Creality Ender-3). Since the system needs to be soft, thin, and very comfortable to fit the clinician's thumb and not compromise the procedure, thermoplastic polyurethane (TPU) was used as a printing filament (JAYO TPU Shore 95 A), as it is a particularly flexible but at the same time resistant elastomer. Before printing, *Ultimaker Cura* software was used to set the optimal printing parameters and to get a preview of the process [see Fig. 2(a)]. The selected printing settings are reported in Table I.

After that, the printing process started [see Fig. 2(b)], by following the steps proposed in [20], [21], [22], and is listed below. Once the groove structure designed to accommodate the FBG was half complete, the printing process was stopped. At this stage, the FBG was prestretched and placed into the host structure [see Fig. 2(c)]. The printing is resumed [see Fig. 2(d)], and the FBG was fully embedded into the 3D

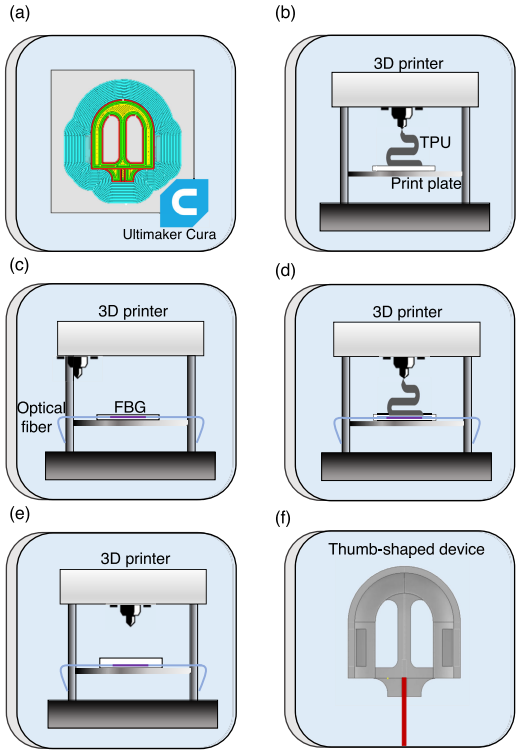

Fig. 2. Steps performed during the fabrication process of the wearable 3D-printed device. (a) Setting of the optimal printing process through *Ultimaker Cura* software. (b) Start of the printing process. (c) Optical fiber pulling and its placement in the grooved channel. (d) Resume of the printing process. (e) End of the printing process. (f) Peeling out of the 3D-printed sensor from the printing plate.

device [see Fig. 2(e)]. The 3D device was peeled out from the print plate [see Fig. 2(f)].

Fig. 3(a) reports the reflected spectrum of the FBG used to develop the thumb-shaped device before (i.e., once it is stretched) and after (i.e., at the end of the printing process) its integration in the TPU material. As can be seen, after the embedding in TPU material, the FBG spectrum experiences a blue shift (left shift of 0.61 nm from 1557.21 to 1556.60 nm). A slight variation in the spectrum shape was found before and post-integration process, as suggested by the calculation of the full width at half maximum (FWHM) [shown as an example in Fig. 3(b)] (i.e., $\text{FWHM}_{\text{before}} = 1.44$ nm and $\text{FWHM}_{\text{after}} = 1.26$ nm).

Finally, an elastic band was sewn in correspondence with the two lateral holes of the device to allow wearability (see Fig. 4).

III. Metrological Characterization

After the fabrication, a metrological characterization of the thumb-shaped device was performed to assess the system's response to force (F).

For this purpose, seven compression tests were performed using a testing machine (model 3365, Instron, Norwood, MA, USA). The wearable thumb-shaped device was placed between the lower plate of the machine and a polylactic acid (PLA)-printed cylinder mold with an internal cavity fitting the machine's indenter and a smaller cylindrical extrusion at its end to exert F directly on the surface embedding the FBG

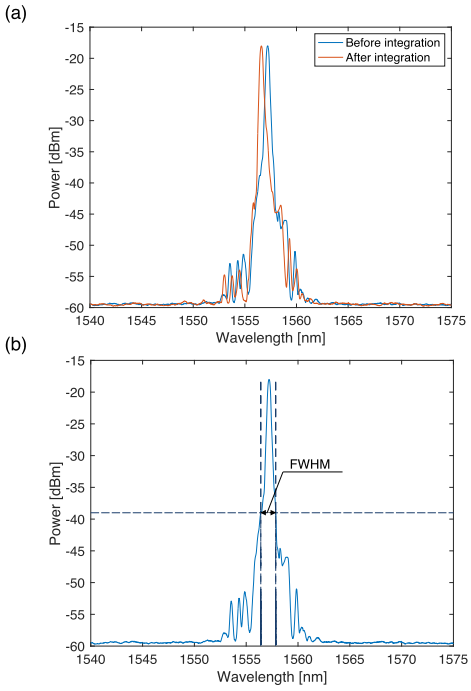

Fig. 3. (a) Reflected spectrum of the FBG sensor used to develop the thumb-shaped device before (continuous blue line) and after integration (continuous orange line). (b) As an example FWHM of the FBG reflected spectrum before integration.

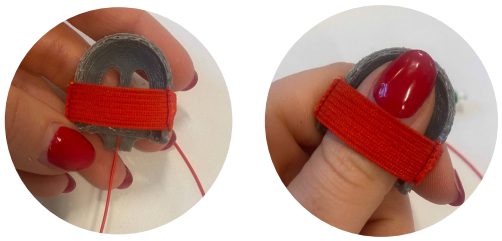

Fig. 4. Thumb-shaped device with the elastic band.

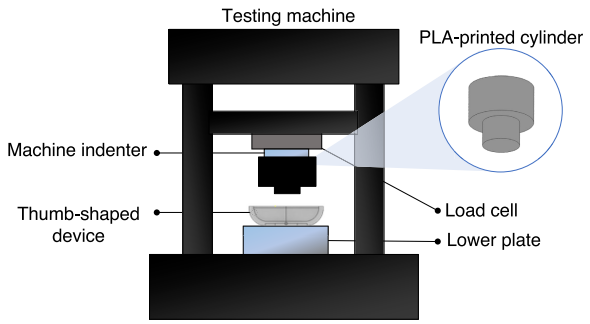

Fig. 5. Positioning of the thumb-shaped device between the lower plate of the testing machine and the PLA-printed cylinder.

sensor (as shown in Fig. 5). During tests, an external F in the range of 0–50 N was applied perpendicular to the surface of the device at a set speed of 2 mm/min, thus mimicking quasi-static conditions. A load cell (full-scale value of 500 N and accuracy of ±0.25% of the reading value, serial number 69 376, Instron, Norwood, MA, USA) allowed acquiring F values at a sampling rate of 100 Hz. At the same time, FBG

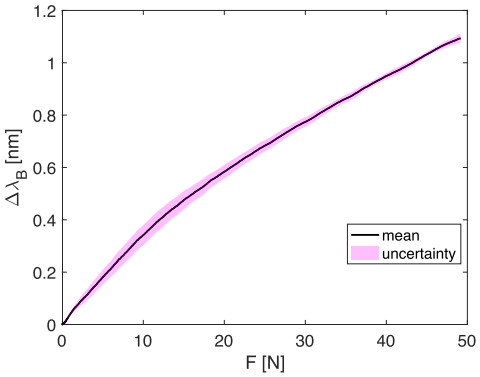

Fig. 6. Average $\Delta\lambda_B$ trend as a function of the applied F and the related uncertainty obtained across the seven compression tests carried out.

output was collected at the same frequency by means of an optical interrogator (si255 Micrometer Optics Inc., USA).

Afterward, $\Delta\lambda_B$ and F values were postprocessed in MATLAB software. The average $\Delta\lambda_B$ trend as a function of the applied F across the seven compression tests was computed with the related uncertainty (see Fig. 6), calculated as follows:

$$\delta_x = k \cdot \frac{S_x}{\sqrt{N}} \tag{3}$$

in which S_x represents the standard deviation, N the numbers of tests performed (i.e., seven), and k the coverage factor. The latter was computed by means of a t-Student distribution with a confidence level of 95% and a number of freedom degrees equal to $N - 1$ (i.e., six). Finally, the mean sensitivity to F (i.e., $S_{F,\text{mean}}$) was calculated in terms of average sensitivity using the following formula [40]:

$$S_{F,\text{mean}} = \frac{\Delta\lambda_B\left(F^{\max}\right) - \Delta\lambda_B\left(F^0\right)}{F^{\max} - F^0} \tag{4}$$

where $\Delta\lambda_B(F^{\max})$ represents $\Delta\lambda_B$ recorded in correspondence with the maximum applied force (i.e., $F^{\max}$) and $\Delta\lambda_B(F^0)$ is the one recorded in correspondence with 0 N (i.e., F^0). The results obtained suggest $S_{F,\text{mean}}$ equal to 0.022 nm $\cdot$ N^{-1}.

Considering the nonlinear behavior of the average $\Delta\lambda_B$ trend versus F curve S_F can also be calculated within two different F ranges (i.e., ~0–25 N and 25–50 N) in which the sensor response can be approximated to a linear trend. In this case, S_F values were retrieved as the slope of the line best fits the experimental data. A S_F value of 0.030 and 0.018 nm $\cdot$ N^{-1} was found in F ranges of ~0–25 and 25–50 N, respectively.

IV. Feasibility Assessment in the Clinical Setting

After metrological characterization, a feasibility assessment in a clinical setting was carried out to evaluate the capability of the proposed system in detecting LOR.

A. Experimental Setup

Tests in a real scenario were performed at our hospital's pain therapy outpatient clinic. Before patients' enrollment,

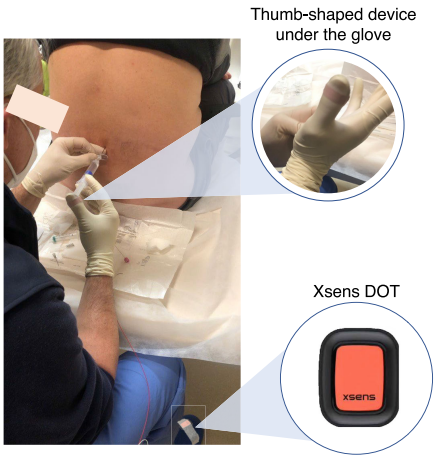

Fig. 7. As an example, one of the two epidural procedures carried out by the anesthesiologist wearing the thumb-shaped device under the glove and the accelerometer attached to his foot.

the study was approved by the Ethical Committee of our institution (Ref: 04.16-OSS). Two patients were recruited in accordance with the guidelines provided by the Declaration of Helsinki and accepted participation by signing informed consent. The same anesthesiologist performed all the procedures and generally used the LOR method with saline solution to detect ES. A total of two tests were carried out on patients affected by low back pain. Epidural punctures occurred in one of the intervertebral spaces, according to the patient's pathology. Before starting the procedure, each patient was asked to take up the fetal position to identify the intervertebral space easily. After preparing the sterile field and placing the Tuohy needle in the affected area, the anesthesiologist wore the thumb-shaped device and put on the sterile glove (see Fig. 7). The proposed device was connected to the optical interrogator throughout the procedure for data acquisition at a sampling rate of 1 kHz. To assess the correspondence between the FBG output and the clinician's LOR perception, a three-axis accelerometer (Xsens DOT, Xsens Technologies B.V) was placed on the anesthesiologist's foot, asking him to tap his foot when he felt the LOR. This resulted in a prominent peak along the three axes of the accelerometer. In this way, it was possible to assess whether the needle passage in the ES, felt by the clinician and tracked by the accelerometer, matches the sudden decrease in $\Delta\lambda_B$ recorded by the thumb-shaped device. Data from the accelerometer were acquired at 60 Hz and stored on a smartphone using the specific app (Xsens DOT Motion Tracking). To mark the start of the procedure, the anesthesiologist was asked to give three initial taps on both the systems.

B. Data Analysis

Data stored during tests were postprocessed in MATLAB environment. The steps performed in data processing are listed below.

1) From the acceleration values recorded along the three axes, the vector magnitude unit (VMU) was calculated, as reported in the following equation:

$$\text{VMU} = \sqrt{a_x^2 + a_y^2 + a_z^2}. \tag{5}$$

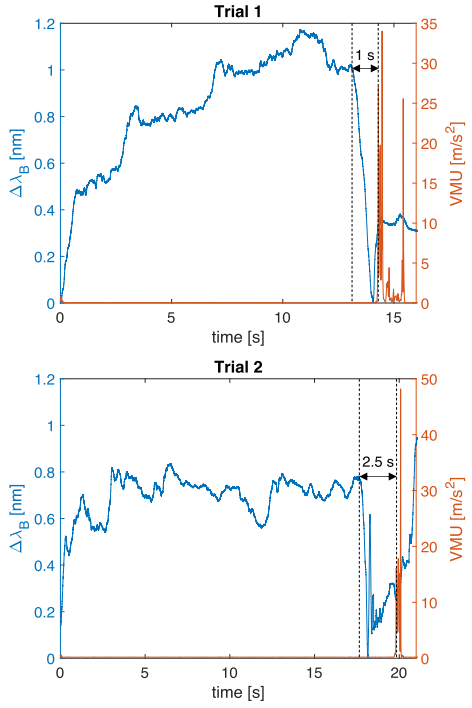

Fig. 8. Results of the two trials performed in a clinical scenario using the proposed thumb-shaped device and the accelerometer. For each subplot, $\Delta\lambda_B$ trend is reported with the continuous blue line, and VMU trend is highlighted with the continuous orange line. The time elapsed between $\Delta\lambda_B$ drop and the perturbation in the VMU signal is also highlighted between two black dashed lines for each plot.

2) $\Delta\lambda_B$ and VMU signals were synchronized, considering as reference the minimum value after the third peak related to the phase in which the anesthesiologist was asked to give three initial taps on both the systems.
3) $\Delta\lambda_B$ were downsampled at the same sampling frequency of the accelerometer signal (i.e., 60 Hz).
4) $\Delta\lambda_B$ and VMU signals were plotted as a function of time. Thus, the elapsed time between the drop in $\Delta\lambda_B$ and the peak in the VMU signal could be assessed.

Moreover, from $\Delta\lambda_B$ values recorded during each procedure, F applied by the operator to allow the needle advancement was calculated considering $S_{F,\text{mean}}$ (i.e., 0.022 nm $\cdot$ N^{-1}) obtained from the metrological characterization process.

C. Results

Fig. 8 reports the results obtained for the two tests carried out reported as subplots (one for each trial). $1\lambda_B$ and VMU signals collected are reported with continuous blue and orange lines for each subplot, respectively. The time elapsed between $\Delta\lambda_B$ drop and the perturbation in the VMU signal is also highlighted between two black dashed lines for each plot.

The output collected from the thumb-shaped device over time showed a similar trend that can be described as follows: 1) a rapid increase in $\Delta\lambda_B$ at the beginning of the procedure; 2) a stage when $\Delta\lambda_B$ values are maintained over a threshold varying according to the amount of force applied by the clinician to cross several tissue layers; and 3) an abrupt drop in $\Delta\lambda_B$ when the needle tip overcomes the ligamentum flavum and hits the ES. The maximum $\Delta\lambda_B$ recorded in each test ranged between 0.8 and 1.2 nm. During the entire procedure, VMU values obtained from the accelerometer signals were around 0 because the physician's foot was firmly planted on the ground. The VMU exhibited an abrupt change when the physician's foot lifted after perceiving the LOR. In Fig. 8, it is clearly visible that peaks in the accelerometer signal occurred immediately after the drop in $\Delta\lambda_B$ signals (i.e., 1 s after in the first trial and 2.5 s after in the second one), suggesting the thumb-shaped device's capability to identify the ES, correctly.

V. Discussions and Conclusion

In this study, we presented a wearable 3D-printed thumb-shaped device based on FBG technology to identify the ES correctly. The 3D printing technique for integrating FBG sensors had not been explored before in this application. Its exploitation improved system customization and robustness while ensuring better repeatability in the manufacturing process, less procedure time, and reduced costs. The proposed device was designed in shape mimicking the human thumb, thus allowing wearability under the operator glove. As a result, the limitations found in other systems previously proposed in the literature have been well-addressed. Indeed, instrumented needles reported in [30], [31], [32], and [33] can obstruct drug passage, resulting in reduced efficacy and suboptimal pain management. In some cases, these solutions require a new needle assembly without any syringe, which totally disrupts the standard procedure and bypasses the clinician's perception [31], [33]. Moreover, such options are hardly applicable in the real scenario since the needle is disposable. The flexible plunger cap for LOR detection proposed by our research group [35], [36] recently has the advantage of not being in direct contact with the tissue and without alteration in the traditional method. However, an appropriate sterilization process is required at each use, thus avoiding the risk of contamination of the sterile field. Instead, the wearable device proposed in this study allowed the prevention of barren infection without obstructing the fluid passage since it is worn directly under the glove. Using TPU material made it possible to develop a highly flexible system without impairing the clinician's tactile sensation during the procedure. In addition, the exploitation of 3D printing enables the development of systems under more controlled conditions and in shorter timescales than processes involving silicone rubbers or resin materials, where the time required to cure the substrate can range from a couple of hours to even a day.

Moreover, the metrological characterization allowed calculating $S_{F,\text{mean}}$ obtaining a value equal to 0.022 nm $\cdot$ N^{-1} in the range of 0–50 N, which covers F applied in this application [41]. Since the calibration curve is not perfectly linear, we also analyzed the sensitivity considering two F ranges: for F ranging between 0 and 25 N, $\Delta\lambda_B$ showed an S_F of 0.030 nm $\cdot$ N^{-1}, while in the range 25–50 N S_F was 0.018 nm $\cdot$ N^{-1}. Even considering this worst value, the thumb-shaped device can detect F drops much lower than the one experienced during the experiments in real settings. Indeed, trials carried out in this study show drops of tens of N (obtained considering $\Delta\lambda_B$ drops reported in Fig. 8 and $S_{F,\text{mean}}$ value), while the system is able to detect F drops

much lower than 1 N. Moreover, it is important to highlight that the geometric parameters (i.e., sizes, FBG positioning), the printing settings (e.g., infill density, and pattern), and the encapsulation material chosen to embed the FBG sensor can cause changes in metrological characteristics of the proposed system [21], [36]. For this reason, further investigations will be carried out to evaluate modifications in the structural design for optimizing the performance of the proposed system in terms of S_F. Beyond that, a deeper insight will be required to gain a deeper insight into the reproducibility of the proposed fabrication process.

Feasibility tests in a real-clinical scenario on two patients affected by low back pain enabled us to assess the capability of the thumb-shaped device in detecting ES. An accelerometer was attached to his foot to relate the clinician's perception to the output of our device. The clinician was instructed to strike on the ground once he perceived the LOR. The results obtained for the two trials showed a perturbation in the accelerometer signal shortly after the drop in $\Delta\lambda_B$, thus suggesting the capability of the proposed device in identifying ES. The time elapsed between the drop in the output of the thumb-shaped sensor once ES is reached and the clinician's perception detected by the accelerometer is within a physiological response window. Therefore, this system has the potential to be a valuable tool for measuring the drop in resistance occurring when ES is reached and breaking away from the traditional LOR approach, thus allowing objectivation of the operator's perceived perception. Although the wearable device showed promising results, additional tests will be necessary to evaluate its effectiveness and ease of use in a larger group of patients with musculoskeletal disorders and pathologies. Also, enrolling operators with different experience levels will lead to a more in-depth evaluation of the device's viability. To avoid false positives due to pressure drops caused by potential needle repositioning during the procedure, an additional FBG sensor could be integrated into the device to detect any thumb lift. In this study, we proposed a system that can be adaptable to different sizes, thanks to the use of an elastic band for wrapping the device around the anesthesiologist's thumb. However, future optimization in the design of the proposed device will be considered to increase its adaptability, accounting for covering a wider variability of the anthropometric characteristics.

REFERENCES

[1] D. L. Presti et al., "Fiber Bragg gratings for medical applications and future challenges: A review," *IEEE Access*, vol. 8, pp. 156863–156888, 2020.

[2] V. Mishra, N. Singh, U. Tiwari, and P. Kapur, "Fiber grating sensors in medicine: Current and emerging applications," *Sens. Actuators A, Phys.*, vol. 167, no. 2, pp. 279–290, Jun. 2011.

[3] M. Mishra and P. K. Sahu, "Fiber Bragg gratings in healthcare applications: A review," *IETE Tech. Rev.*, vol. 40, no. 2, p. 202–219, 2022.

[4] A. Leal-Junior et al., "Fiber Bragg gratings in CYTOP fibers embedded in a 3D-printed flexible support for assessment of human–robot interaction forces," *Materials*, vol. 11, no. 11, p. 2305, Nov. 2018.

[5] C. Broadway, R. Min, A. G. Leal-Junior, C. Marques, and C. Caucheteur, "Toward commercial polymer fiber Bragg grating sensors: Review and applications," *J. Lightw. Technol.*, vol. 37, no. 11, pp. 2605–2615, Jun. 1, 2019.

[6] Y.-J. Rao, D. J. Webb, D. A. Jackson, L. Zhang, and I. Bennion, "Optical in-fiber Bragg grating sensor systems for medical applications," *J. Biomed. Opt.*, vol. 3, no. 1, pp. 38–44, 1998.

[7] Z. Tang, S. Wang, M. Li, and C. Shi, "Development of a distal tri-axial force sensor for minimally invasive surgical palpation," *IEEE Trans. Med. Robot. Bionics*, vol. 4, no. 1, pp. 145–155, Feb. 2022.

[8] S. Li et al., "Band-rejection feedback for chaotic time-delay signature suppression in a semiconductor laser," *IEEE Photon. J.*, vol. 14, no. 2, pp. 1–8, Apr. 2022.

[9] A. Prasad, S. Pant, S. Srivatzen, and S. Asokan, "A non-invasive breast cancer detection system using FBG thermal sensor array: A feasibility study," *IEEE Sensors J.*, vol. 21, no. 21, pp. 24106–24113, Nov. 2021.

[10] D. L. Presti et al., "Wearable system based on flexible FBG for respiratory and cardiac monitoring," *IEEE Sensors J.*, vol. 19, no. 17, pp. 7391–7398, Sep. 2019.

[11] L. Dziuda, J. Lewandowski, F. Skibniewski, and G. Nowicki, "Fibre-optic sensor for respiration and heart rate monitoring in the MRI environment," *Proc. Eng.*, vol. 47, pp. 1291–1294, Jan. 2012.

[12] F. De Tommasi, D. L. Presti, M. A. Caponero, M. Carassiti, E. Schena, and C. Massaroni, "Smart mattress based on multipoint fiber Bragg gratings for respiratory rate monitoring," *IEEE Trans. Instrum. Meas.*, vol. 72, pp. 1–10, 2023.

[13] A. G. Leal-Junior, V. Campos, C. Díaz, R. M. Andrade, A. Frizera, and C. Marques, "A machine learning approach for simultaneous measurement of magnetic field position and intensity with fiber Bragg grating and magnetorheological fluid," *Opt. Fiber Technol.*, vol. 56, May 2020, Art. no. 102184.

[14] M. Fajkus, J. Nedoma, P. Siska, and V. Vasinek, "FBG sensor of breathing encapsulated into polydimethylsiloxane," *Proc. SPIE*, vol. 9994, pp. 31–35, Oct. 2016.

[15] Z. A. Abro, Y.-F. Zhang, C.-Y. Hong, R. A. Lakho, and N.-L. Chen, "Development of a smart garment for monitoring body postures based on FBG and flex sensing technologies," *Sens. Actuators A, Phys.*, vol. 272, pp. 153–160, Apr. 2018.

[16] M. Rocha, C. Tavares, C. Nepomuceno, P. F. d. C. Antunes, M. de Fátima Domingues, and N. J. Alberto, "FBGs based system for muscle effort monitoring in wheelchair users," *IEEE Sensors J.*, vol. 22, no. 13, pp. 12886–12893, Jul. 2022.

[17] S. He, S. Feng, A. Nag, N. Afsarimanesh, T. Han, and S. C. Mukhopadhyay, "Recent progress in 3D printed mold-based sensors," *Sensors*, vol. 20, no. 3, p. 703, Jan. 2020.

[18] Y. Xu et al., "The boom in 3D-printed sensor technology," *Sensors*, vol. 17, no. 5, p. 1166, May 2017.

[19] M. R. Khosravani and T. Reinicke, "3D-printed sensors: Current progress and future challenges," *Sens. Actuators A, Phys.*, vol. 305, Apr. 2020, Art. no. 111916.

[20] C. Tavares et al., "Respiratory and heart rate monitoring using an FBG 3D-printed wearable system," *Biomed. Opt. Exp.*, vol. 13, no. 4, pp. 2299–2311, 2022.

[21] D. L. Presti et al., "The effect of infill pattern and density on the response of 3-D-printed sensors based on FBG technology," *IEEE Sensors J.*, vol. 22, no. 20, pp. 19357–19365, Oct. 2022.

[22] A. G. Leal-Junior, C. Marques, M. R. N. Ribeiro, M. J. Pontes, and A. Frizera, "FBG-embedded 3-D printed ABS sensing pads: The impact of infill density on sensitivity and dynamic range in force sensors," *IEEE Sensors J.*, vol. 18, no. 20, pp. 8381–8388, Oct. 2018.

[23] Z. Hao, K. Cook, J. Canning, H. Chen, and C. Martelli, "3-D printed smart orthotic insoles: Monitoring a Person's gait step by step," *IEEE Sensors Lett.*, vol. 4, no. 1, pp. 1–4, Jan. 2020.

[24] M. Carassiti et al., "Epidural steroid injections for low back pain: A narrative review," *Int. J. Environ. Res. Public Health*, vol. 19, no. 1, p. 231, 2022.

[25] R. J. Moraca, D. G. Sheldon, and R. C. Thirlby, "The role of epidural anesthesia and analgesia in surgical practice," *Ann. Surgery*, vol. 238, no. 5, pp. 663–673, 2003.

[26] S. Fyneface-Ogan, "Anatomy and clinical importance of the epidural space," *Epidural Analgesia-Current Views Approaches*, vol. 12, pp. 1–12, Mar. 2012.

[27] S. Segal and K. W. Arendt, "A retrospective effectiveness study of loss of resistance to air or saline for identification of the epidural space," *Anesthesia Analgesia*, vol. 110, no. 2, pp. 558–563, 2010.

[28] A. Thangamuthu, I. F. Russell, and M. Purva, "Epidural failure rate using a standardised definition," *Int. J. Obstetric Anesthesia*, vol. 22, no. 4, pp. 310–315, Nov. 2013.

[29] W. Ruppen, S. Derry, H. McQuay, and R. A. Moore, "Incidence of epidural hematoma, infection, and neurologic injury in obstetric patients with epidural analgesia/anesthesia," *Anesthesiology*, vol. 105, no. 2, pp. 394–399, Aug. 2006.

[30] B. Carotenuto et al., "Optical guidance systems for epidural space identification," *IEEE J. Sel. Topics Quantum Electron.*, vol. 23, no. 2, pp. 371–379, Mar. 2017.
[31] B. Carotenuto et al., "Optical fiber technology enables smart needles for epidurals: an in-vivo swine study," *Biomed. Opt. Exp.*, vol. 10, no. 3, pp. 1351–1364, 2019.
[32] A. Amantayeva, N. Adilzhanova, A. Issatayeva, W. Blanc, C. Molardi, and D. Tosi, "Fiber optic distributed sensing network for shape sensing-assisted epidural needle guidance," *Biosensors*, vol. 11, no. 11, p. 446, Nov. 2021.
[33] S. Ambastha, S. Umesh, S. Dabir, and S. Asokan, "Spinal needle force monitoring during lumbar puncture using fiber Bragg grating force device," *J. Biomed. Opt.*, vol. 21, no. 11, Nov. 2016, Art. no. 117002.
[34] F. de Tommasi, D. L. Presti, C. Massaroni, E. Schena, and M. Carassiti, "FBG-based system for loss of resistance detection during epidural injections," in *Proc. IEEE Int. Workshop Metrol. Ind. 4.0 IoT (MetroInd4.0&IoT)*, Jun. 2021, pp. 172–176.
[35] F. D. Tommasi, D. L. Presti, F. Virgili, C. Massaroni, E. Schena, and M. Carassiti, "Soft system based on fiber Bragg grating sensor for loss of resistance detection during epidural procedures: In silico and in vivo assessment," *Sensors*, vol. 21, no. 16, p. 5329, Aug. 2021.
[36] F. De Tommasi, C. Romano, D. L. Presti, C. Massaroni, M. Carassiti, and E. Schena, "FBG-based soft system for assisted epidural anesthesia: Design optimization and clinical assessment," *Biosensors*, vol. 12, no. 8, p. 645, Aug. 2022.
[37] T. Erdogan, "Fiber grating spectra," *J. Lightw. Technol.*, vol. 15, no. 8, pp. 1277–1294, Aug. 1997.
[38] D. H. Kang, S. O. Park, C. S. Hong, and C. G. Kim, "The signal characteristics of reflected spectra of fiber Bragg grating sensors with strain gradients and grating lengths," *NDT E Int.*, vol. 38, no. 8, pp. 712–718, Dec. 2005.
[39] F. De Tommasi et al., "Fiber Bragg gratings for temperature measurements under thermal gradients: Comparison between two different lengths," *IEEE Trans. Instrum. Meas.*, early access, May 15, 2023, doi: 10.1109/TIM.2023.3276511.
[40] K. Xu, "Silicon electro-optic micro-modulator fabricated in standard CMOS technology as components for all silicon monolithic integrated optoelectronic systems," *J. Micromech. Microeng.*, vol. 31, no. 5, May 2021, Art. no. 054001.
[41] L. L. H. Holton, "Force models for needle insertion created from measured needle puncture data," in *Medicine Meets Virtual Reality 2001*. Amsterdam, The Netherlands: IOS Press, 2001, pp. 180–186.

Francesca De Tommasi (Student Member, IEEE) received the M.Sc. degree in biomedical engineering from the Università Campus Bio-Medico di Roma (UCBM), Rome, Italy, in 2020, where she is currently pursuing the Ph.D. degree in bioengineering.

Her research interests include development of FBG-based measurement systems for medical treatments and diagnosis.

Carlo Massaroni (Senior Member, IEEE) received the Ph.D. degree in biomedical engineering from UCBM, Rome, Italy, in 2017.

He is currently an Assistant Professor with UCBM. His research interests include design, development, and testing of wearable devices and contactless techniques, methods, and measuring systems for medical applications.

Michele Arturo Caponero received the bachelor's degree in physics from the University of Bari, Bari, Italy, in 1986.

He is a Researcher with the Photonics Micro and Nanostructures Laboratory, ENEA Frascati Research Center, Frascati, Rome, Italy. His research interests include distributed fiber-optic-based sensors for structural monitoring and interferometric technique's development.

Emiliano Schena (Senior Member, IEEE) received the Ph.D. degree in biomedical engineering from UCBM, Rome, Italy, in 2009.

He is currently an Associate Professor with UCBM. His main research interests include systems for monitoring physiological parameters, application of fiber optic sensors in medicine, and laser ablation for cancer removal.

Daniela Lo Presti (Member, IEEE) received the Ph.D. degree from UCBM, Rome, Italy, in 2021.

She is currently an Assistant Professor with the Unit of Measurements and Biomedical Instrumentation, UCBM. Her main research interests include design, fabrication, and feasibility assessment of smart systems and wearables based on fiber optics technology for biomedical applications.

Massimiliano Carassiti received the Ph.D. degree from the University of Navarra, Pamplona, Spain, in 1994.

He is currently Anesthesiologist with Fondazione Policlinico Universitario Campus Bio-Medico di Roma (UCBM), Rome, Italy, and an Assistant Professor at UCBM. His main clinical and research interests include anesthesiology, intensive care medicine, pain medicine, and management.

Open Access funding provided by 'Università "Campus Bio-Medico" di Roma' within the CRUI CARE Agreement